

# Short Slots as Resonance Tuning Elements in Rectangular ENZ Waveguides

Nebojša Vojnović, Branka Jokanović, Miloš Radovanović

**Abstract –** In this paper we present novel methods for tuning of resonances arising in rectangular ENZ waveguides. This kind of tuning is achieved using short longitudinal and inclined slots placed in the ENZ channel. It is shown that using this technique it is possible to tune the tunneling and Fabry-Perot resonances simultaneously by 9.3% and 4.2%, respectively. Also, it is possible to tune these resonances independently: the tunneling frequency by 4.5% and Fabry-Perot resonances by 12.6%. In addition, equivalent circuits for the considered slot orientations are demonstrated along with the corresponding extracted parameters. Analytical expression for longitudinal slot reactance is derived and a very good agreement with the extracted values is observed.

**Keywords –** Epsilon-near-zero (ENZ) waveguide, waveguide slots, equivalent circuits, frequency tuning.

## I. INTRODUCTION

Metamaterials have become very popular in the scientific community in the recent years due to the possibility of synthesizing their constitutive parameters  $\epsilon$  and  $\mu$  with a high degree of freedom including both negative as well as values close to zero. This aspect opened a wide range of possible metamaterial applications in microwave and optical frequency domains.

It is interesting to mention that the dispersion characteristics of a rectangular waveguide operating near the fundamental mode cut-off frequency was utilized in [1] for the first time as a possibility of realizing epsilon-near-zero (ENZ) metamaterials. These waveguide structures are especially interesting due to the simple construction compared to their microstructured counterparts.

The main property of ENZ waveguide structures which made them extremely popular is, in fact, their inherent ability to "squeeze" and tunnel electromagnetic (EM) energy through very tight waveguide channels. When conditions for such tunneling are met, EM energy travels in a static-like fashion with infinite guided wavelength and without phase delay along the channel. Theoretical discussions about these seemingly anomalous phenomena can be found in [2], and experimental verification is given in [3].

Since the tunneling condition is met only at one specific frequency, it would be very convenient if one could tune the tunneling frequency in order to meet different specifications. Reports on this sort of tuning are very scarce, so an easy and effective way of tuning the tunneling frequency is yet to be found. In [4] the tunneling frequency of the ENZ waveguide structure was altered using a varactor diode in the middle of the channel accompanied by an appropriate biasing network.

The authors are with the Institute of Physics, University of Belgrade, Pregrevica 118, 11080 Belgrade, Serbia (e-mail: nebojsav@ipb.ac.rs, brankaj@ipb.ac.rs, rmilos@ipb.ac.rs)

However, this method is not easy to apply to the ENZ structures with thinner channels. In a recent paper published by our group [5], two longitudinal non-resonant slots were placed at the channel inputs as elements for simultaneous tuning of ZOR (zeroth-order-resonance) and *Fabry-Perot* resonances of the considered structure. Theoretical results were also confirmed experimentally.

In this paper we present methods for tuning of resonances in the ENZ channel. Since more than one resonance can occur in ENZ waveguide structures, it would be significant from the application's point of view if one could tune not only both resonances simultaneously, but every resonance separately from the others. We also present equivalent circuits for ENZ waveguides with slots used for tuning the resonances along with the extracted slot parameters and analytical expressions for the longitudinal slots versus frequency. All the considered slots are very short compared to the free-space wavelength and analytical expressions describing their impedances cannot be found in the literature. This paper is organized as follows: after the introduction, a description of the initial structure is given in Sec. II. In Sec. III, IV and V three methods for resonance tuning in the ENZ channel using longitudinal and inclined slots are described and an extraction method is derived in order to calculate the slot impedances. Finally, the conclusions are drawn in Sec. VI.

## II. ENZ WAVEGUIDE - INITIAL STRUCTURE

The ENZ waveguide considered in this paper consists of two input waveguides and a thin channel placed between them and is intended for application in 8 - 16 GHz frequency range. It is depicted in Fig. 1 along with all of its relevant dimensions. Metallization and segments filled with different dielectrics are clearly visible. Waveguide ports are placed on the leftmost and rightmost sides of the structure.

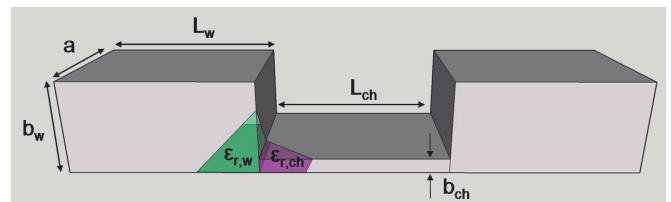


Fig. 1. Initial ENZ waveguide structure; widths and heights of input waveguides are  $a=7.62$  mm and  $b_w=4.064$  mm, respectively, height of the channel is  $b_{ch}=0.254$  mm and lengths of both waveguides and channel are  $L_w=L_{ch}=7$  mm

Permittivities of the dielectrics filling the waveguide sections have real values  $\epsilon_{rw}=6$  and  $\epsilon_{rch}=3$  (losses are not considered) and their values are chosen to fulfill the condition for the tunneling of EM energy stated as [6]:

$$f_w^{TE_{10}} \leq f_{ch}^{TE_{10}} \leq f_w^{TE_{20}} \Rightarrow \frac{\epsilon_{r,w}}{4} \leq \epsilon_{r,ch} \leq \epsilon_{r,w}, \quad (1)$$

where  $f_w^{TE_{10}}$  and  $f_w^{TE_{20}}$  are the cut-off frequencies of the TE<sub>10</sub> and TE<sub>20</sub> modes in input waveguides, respectively. In other words, since the cut-off frequency of the fundamental mode is larger in the channel than in the input waveguides (due to  $\epsilon_{rw} > \epsilon_{rch}$ ), ZOR tuning range is limited by the bandwidth of the input waveguides, i.e. by the frequency range between the fundamental and the next propagating mode.

The equivalent circuit of this structure is given in Fig. 2.

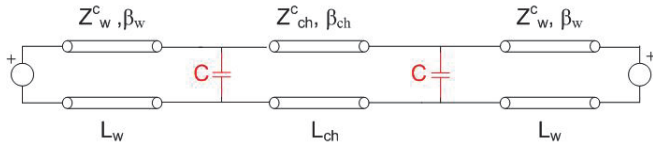


Fig. 2. Equivalent circuit for the structure in Fig. 1. Shunt capacitance  $C$  represents E-plane step between the input waveguide and the channel

$Z_w^c$  and  $Z_{ch}^c$  denote characteristic impedances of the input waveguide and channel, respectively, while  $\beta_w$  and  $\beta_{ch}$  denote the propagation constants in those waveguide sections. Shunt capacitance models the abrupt E-plane step between the input waveguides and the channel according to the expressions given in [7]. Characteristic impedances of the equivalent transmission lines are calculated as:

$$Z_{w(ch)}^c = \frac{2b_{w(ch)}}{a} Z_{w(ch)}^w = \frac{2b_{w(ch)}}{a} \frac{\omega\mu}{\sqrt{\omega^2 \mu_0 \epsilon_0 \epsilon_{r,w(ch)} - (\pi/a)^2}}, \quad (2)$$

where  $Z_{w(ch)}^c$  denotes the characteristic impedance, while  $Z_{w(ch)}^w$  denotes the wave impedance of the TE<sub>10</sub> mode in the input waveguide (channel).

The extraction method presented here implies solving the equivalent circuit from Fig. 2 in order to obtain a closed-form expression for the  $S_{II}$ -parameter (since there is only one unknown element,  $C$ ). Solving the circuit from Fig. 2 is relatively simple using the well-known relation for the input impedance of the transmission line terminated with an arbitrary load:

$$Z_{in} = Z_0 \frac{Z_L + jZ_0 \tan \beta L}{Z_0 + jZ_L \tan \beta L}, \quad (3)$$

where  $Z_L$  denotes the load impedance terminating the line, while  $\beta$  and  $L$  denote the phase coefficient and line length, respectively. After the analytical expression is obtained, the value of the  $S_{II}$ -parameter can be compared with the 3D EM simulation and, based on that comparison, the unknown parameter can be found.

The extraction method presented here is validated by

comparing the values of shunt capacitance  $C$  in Fig. 2, calculated using the expressions from [7] and those obtained using the extraction method. The results are shown in Fig. 3 for three different heights of the channel,  $b_{ch}$ . We can see that at higher frequencies the agreement is very good, while at lower frequencies, typically below the cut-off of the fundamental mode in the channel, the agreement is significantly worse. We can also observe that the agreement between the extracted and calculated capacitances improves for larger  $b_{ch}$ . This was expected bearing in mind that the expressions in [7] were derived for the standard waveguide geometry, i.e. for the case  $a=2b_{ch}$ . Ansys HFSS [8] was used as a full-wave electromagnetic solver throughout this paper.

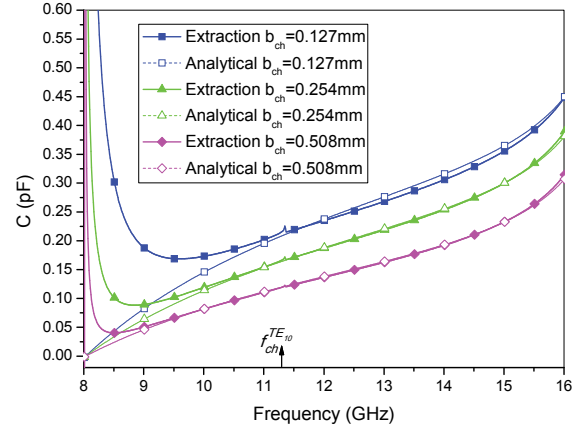


Fig. 3. Extracted capacitances versus capacitances calculated using analytical expressions [7] for three different channel heights,  $b_{ch}$

Simulated  $S$ -parameters of the structure from Fig. 1 and  $S$ -parameters calculated using the extracted values of the shunt capacitance from Fig. 3 are compared in Fig. 4.

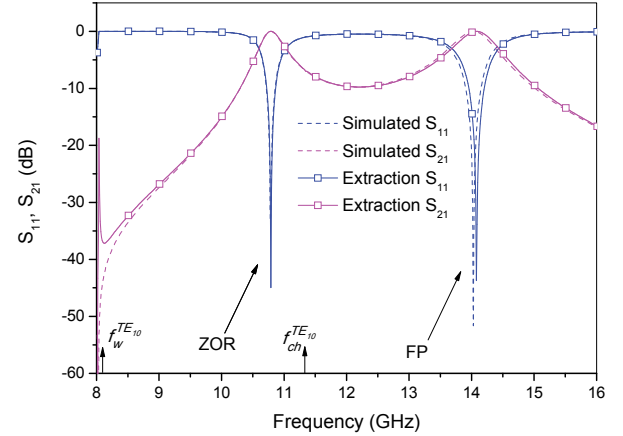


Fig. 4. Simulated and extracted  $S$ -parameters of the initial structure

Fig. 4 shows that the results agreement is very good with the maximum observed error of 0.4% at high frequencies around the FP resonance. This error mainly occurs due to the convergence issues of the 3D solver. As described in [9], the equivalent circuit from Fig. 2 can be analytically solved and resonance conditions can be obtained in closed form. It should be noted that in terms of the equivalent circuit of the ENZ waveguide from Fig. 2, there is no difference between the two

mentioned resonances, i.e. the input impedance matching conditions at resonance are the same for all resonances.

Fig. 5 shows the surface current distributions along the ENZ channel at both resonances.

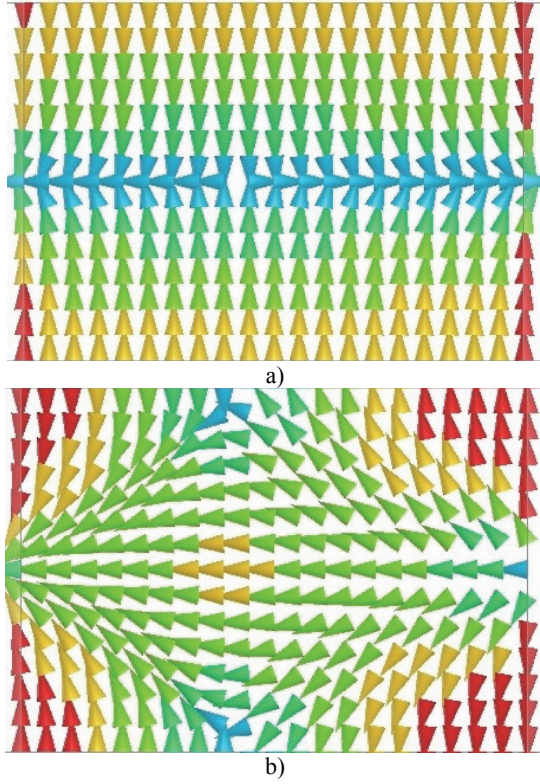


Fig. 5. Surface current density vector along the ENZ channel at a) ZOR and b) FP resonance

### III. ENZ CHANNEL WITH TWO LONGITUDINAL SLOTS

Fig. 6 illustrates the ENZ channel with two non-resonant longitudinal slots cut at the channel inputs. Slot length and width are denoted as  $a_s$  and  $b_s$ , respectively, while its offset from the channel center line is  $d$ . Equivalent circuit that describes the 3D model from Fig. 6 is depicted in Fig. 7.

Longitudinal slots were modeled using shunt reactive elements considering the slots in this configuration intercept the transversal component of the surface current distribution along the ENZ channel. After the extraction procedure it was realized that these reactive elements are in fact capacitive by nature. The real parts of the shunt elements were neglected bearing in mind that the whole structure was considered lossless, and also assuming negligible radiation losses. The equivalent transmission line modeling the channel had to be split into three sections because the slot equivalent parameters (shunt capacitances) must be placed in each slot centre. Hence,  $L_{ch1}$  denotes the distance between the E-plane step and the middle of the neighbouring slot, while  $L_{ch2}$  denotes the distance between the two slot centres.

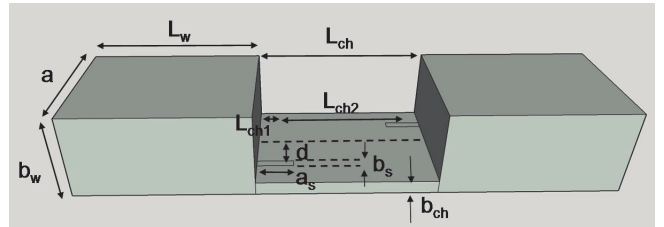


Fig. 6. ENZ channel with two longitudinal slots cut at channel inputs on opposite sides of channel centerline. Slot length and width are  $a_s=3$  mm,  $b_s=0.2$  mm, respectively

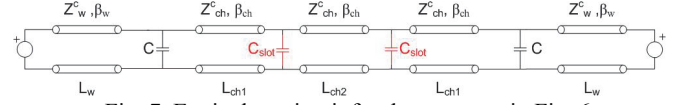


Fig. 7. Equivalent circuit for the structure in Fig. 6

Fig. 8 shows the influence of slot offset on both resonances. Slot length and width were taken as  $a_s=3$  mm (around  $\lambda_0/8$  at central frequency) and  $b_s=0.2$  mm, respectively.

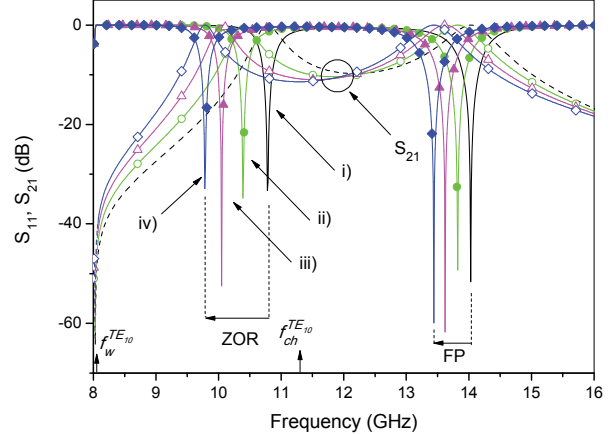


Fig. 8. Influence of slot offset on ZOR and FP ( $a_s=3$  mm,  $b_s=0.2$  mm). i)  $S_{11}$ , no slots, ii)  $S_{11}$ , offset 1.4 mm, iii)  $S_{11}$ , offset 2.1 mm, iv)  $S_{11}$ , offset 2.8 mm;  $S_{21}$  curves are denoted using dashed lines with appropriate symbols

From Fig. 8 it can be seen that placing two symmetrically offset longitudinal slots at channel inputs affects both ZOR and FP resonance. It is understood that two slots positioned in this manner intercept the transversal component of the surface current at both resonances, which in turn produces a resonant frequency shift towards the lower frequencies. The greatest frequency shift for the given slot length observed at ZOR is 9.3% which is accompanied by a 4.2% shift at FP resonance (compared to the case with no slots). Greater frequency shifts can be obtained by increasing slot length [5].

Since the extraction method used for obtaining the slot capacitance throughout this paper inevitably requires a 3D simulation in the whole frequency range of interest, it would be convenient if one could calculate those capacitances using analytical expressions based on only single frequency simulation. In this manner, a great amount of time and computational effort can be saved.

Fig. 9 shows the extracted values of shunt capacitances,  $C_{slot}$ , from Fig. 7, for four different offsets.

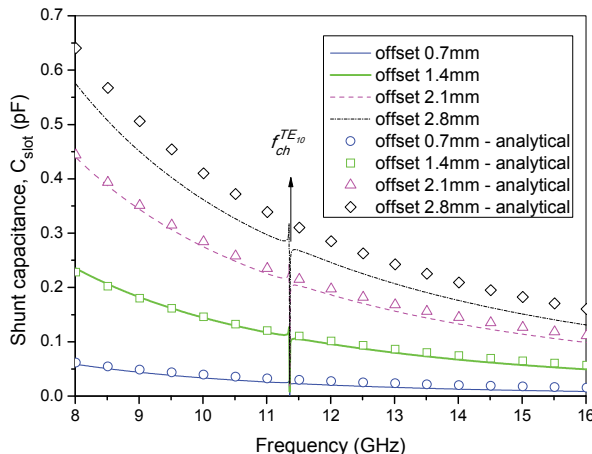


Fig. 9. Frequency dependence of the extracted slot shunt capacitance for four different slot offsets. Extracted values are compared with those obtained analytically using Eq. (4)

As observed from Fig. 9, all the extracted capacitances decay in an exponential fashion and larger offsets yield greater capacitances. The discontinuity at 11.36 GHz is due to the fundamental mode cut-off in the channel.

Fig. 9 also shows the values of capacitances calculated using closed-form analytical expression stated as:

$$C_{slot} = C_0 \left( \frac{f_0}{f} \right)^2 \frac{\sin^2(\pi d)}{\sin^2(\pi d_0)} , \quad b_{ch} = const. \quad (4)$$

with  $C_0$  being the capacitance  $C_{slot}$  extracted at the frequency  $f_0$  for the slot offset  $d_0$ . It was found that  $f_0$  should be chosen near the ZOR resonance. Parameter  $d_0$  was taken to be equal to 50% of the maximum slot offset, i.e. 1.9 mm. The agreement observed in Fig. 9 is very good except in the case when the slot offset is equal to 2.8 mm. This is a consequence of the large coupling between the slot itself and the waveguide sidewall. It should be noted that the each "analytical" curve from Fig. 9 was calculated using a full-wave simulation at only one frequency point.

Since the considered ENZ structure is simulated as lossless, an expression of the form:

$$\rho = 1 - |S_{11}|^2 - |S_{21}|^2 \quad (5)$$

could be interpreted as a measure of power radiated through the slots in the channel, i.e. radiation losses. Fig. 10 shows the  $\rho$  parameter for different slot offsets. Radiated power is greater for greater offsets, which was expected. It is interesting to notice that the radiation, although rather small since the  $\rho$  parameter is of the order of  $10^{-3}$ , is pronounced at both ZOR and FP resonance, but more at FP since the slot electrical length is greater at higher frequencies.

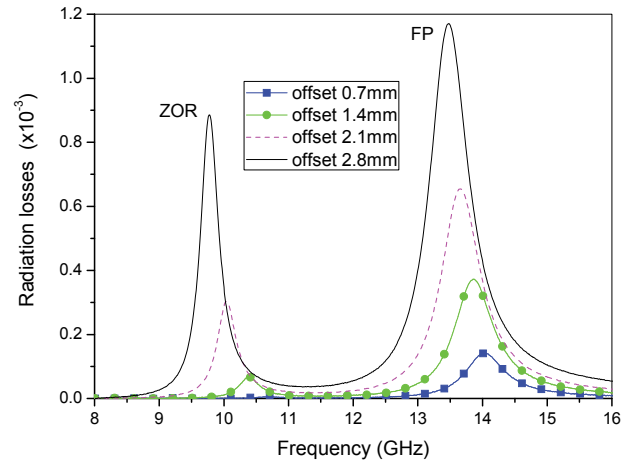


Fig. 10. Dependence of radiation losses on the slot offset

#### IV. ENZ CHANNEL WITH A CENTERED LONGITUDINAL SLOT

As mentioned before, from the application's point of view it would be very convenient to be able to manipulate the position of one waveguide ENZ resonance without influencing the other one. In order to investigate such a possibility, configuration given in Fig. 11 was examined. It consists of a basic ENZ structure from Fig. 1 with the addition of a single centered longitudinal slot with a variable offset.

Fig. 12 depicts the equivalent circuit corresponding to the structure in Fig. 11. Longitudinal slot was modeled using a shunt capacitor, similarly as in the previous section. Real part was once again neglected from the same reasons stated earlier.

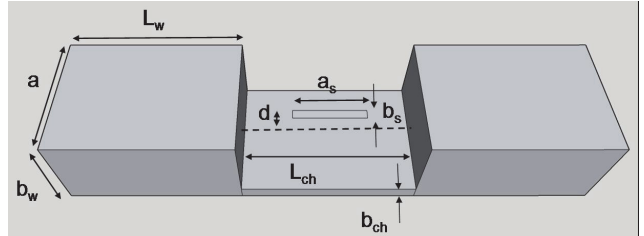


Fig. 11. ENZ channel with a single longitudinal slot in the middle of the channel and offset  $d$ ; length, width and slot offset are denoted with  $a_s$ ,  $b_s$  and  $d$ , respectively. Slot length and width are  $a_s=3$  mm,  $b_s=0.2$  mm, respectively

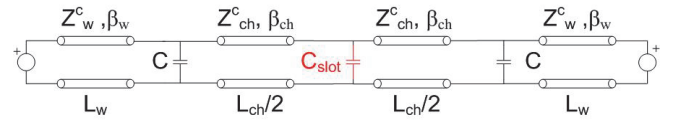


Fig. 12. Equivalent circuit corresponding to Fig. 11

Fig. 13 illustrates the influence of a single slot offset on both resonances. Slot length and width were taken as  $a_s=3$  mm (around  $\lambda_0/8$  at central frequency) and  $b_s=0.2$  mm, respectively. As Fig. 13 shows, placing a single longitudinal slot on the top surface of the ENZ channel results in a frequency shift of ZOR only and not of FP resonance. In other words, with this slot configuration an independent tuning of the tunneling frequency can be achieved. As the slot offset is increased, the tunneling frequency tends towards lower

frequencies while the FP resonance remains at the same frequency. The largest frequency shift for the given slot length is observed for the slot offset of 2.8 mm and is equal to 4.5% compared to the case with no slots.

The same qualitative effect of lowering ZOR can be achieved by increasing the length of the longitudinal slot while keeping its offset fixed as shown in [10].

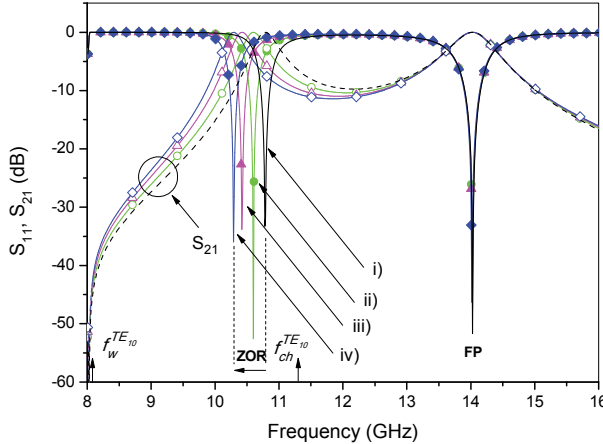


Fig. 13. Influence of a single centered slot offset on ZOR and FP resonance ( $a_s=3$  mm,  $b_s=0.2$  mm). i)  $S_{11}$ , no slots, ii)  $S_{11}$ , offset 1.4 mm, iii)  $S_{11}$ , offset 2.1 mm, iv)  $S_{11}$ , offset 2.8 mm;  $S_{21}$  curves are denoted using dashed lines with appropriate symbols

Fig. 14 shows the extracted values of shunt capacitances for four different offsets of a single centered slot in the channel.

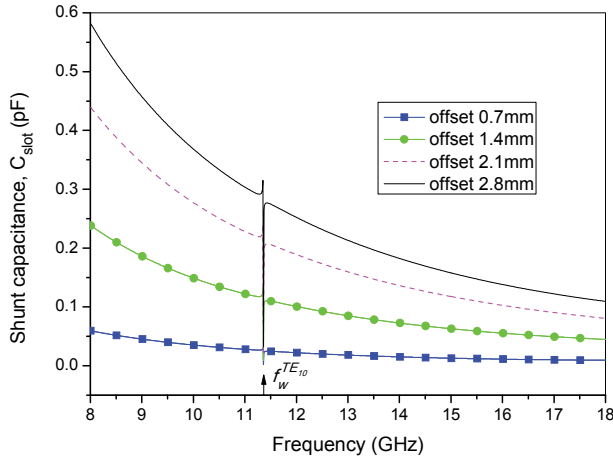


Fig. 14. Frequency dependence of the extracted slot shunt capacitance for four different centered slot offsets

After inspecting Figs. 9 and 14 one concludes that slot capacitances for the longitudinal slot placed at the channel input and for one centered slot (for the same slot length and offset) are identical. In other words, slot capacitance doesn't depend on slot position along the channel and is affected only by the slot length and offset. Hence the results obtained using Eq. (4) will be omitted from Fig. 14.

Analogous to the previous section,  $\rho$  is plotted against frequency in Fig. 15, with slot offset as a parameter. It can be observed that the radiation losses are pronounced only at ZOR and not at FP resonance. After comparing Figs. 10 and 15, it can be seen that one centered longitudinal slot has larger

radiation losses than two slots placed at channel inputs (slots in both cases have the same dimensions and offsets). This is a consequence of different surface current density at the channel inputs and center as observed from Fig. 5.

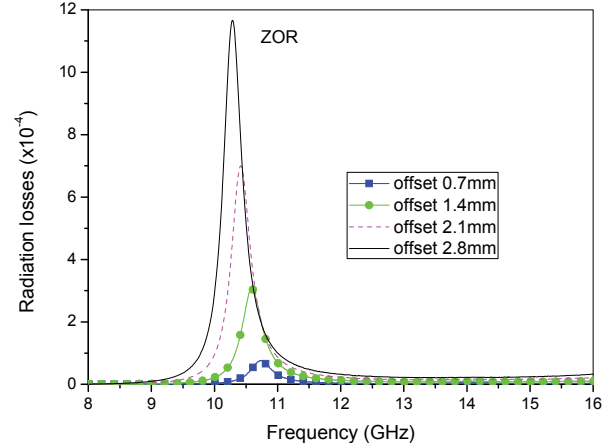


Fig. 15. Dependence of radiation losses on the centered slot offset

## V. ENZ CHANNEL WITH A CENTERED INCLINED SLOT

As was shown in the previous section, placing a single offset longitudinal slot in the ENZ channel is an effective way of tuning the position of the tunneling frequency while the FP resonance retains its position. With that in mind, it would be very convenient if one could also manipulate the position of the FP resonance without influencing the ZOR. In order to further analyze such a possibility, we examine the ENZ structure with a single centered slot with no offset, but instead with an angle of inclination  $\varphi$  relative to the channel longitudinal axes, depicted in Fig. 16.

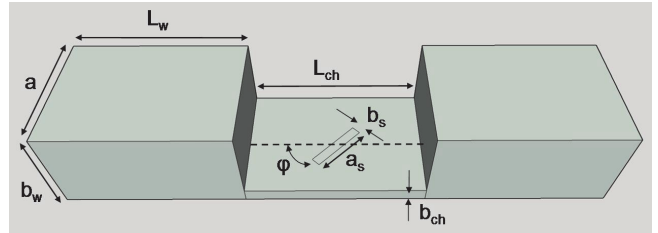


Fig. 16. ENZ channel with a centered inclined slot cut in the middle of the channel top side. Slot length and width are  $a_s=5$  mm,  $b_s=0.2$  mm, respectively

Equivalent circuit corresponding to Fig. 16 is given in Fig. 17. Slot configuration from Fig. 16 intercepts the axial component of the surface current density, hence the inclined slot is modeled by means of a series reactive element (after the extraction it was found that this element has inductive nature). Real part was again neglected.

Fig. 18 illustrates the influence of centered slot angle of inclination on both resonances. Slot length and width were taken as  $a_s=5$  mm (around  $\lambda_0/5$  at central frequency) and  $b_s=0.2$  mm, respectively. As shown in Fig. 18, placing a single centered inclined slot on the top surface of the ENZ channel results in a frequency shift of the FP resonance only and not of ZOR. As the slot angle of inclination is increased, the FP

resonant frequency tends towards lower frequencies while the tunneling frequency remains the same. The largest frequency shift for the given slot length is observed for the slot angle of  $80^\circ$  and is equal to 12.6% when compared to the case without the slot.  $S$ -parameters for the case of the slot angle of inclination equal to  $90^\circ$  are identical compared with the case of the angle equal to  $80^\circ$  and hence will be omitted. Increasing the angle beyond  $90^\circ$  has no significance due to symmetry. Analogous to the comments given in the previous section, lowering the FP resonance can also be achieved by changing the length of the inclined slot while keeping the slot angle of inclination intact.

After considering the results from this and the previous section, it becomes clear that both resonances can be tuned separately by using different orientations of slot placed on the channel top side.

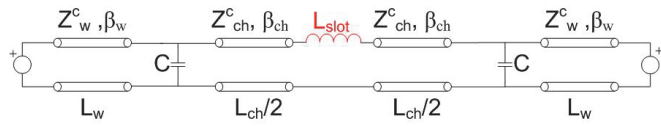


Fig. 17. Equivalent circuit corresponding to Fig. 16

In Fig. 19 the extracted values of the series inductances are given for four different angles of inclination. As this angle increases, the series inductances also increase. We can also observe a slight exponential growth of these inductances with frequency, which is especially pronounced for larger angles.

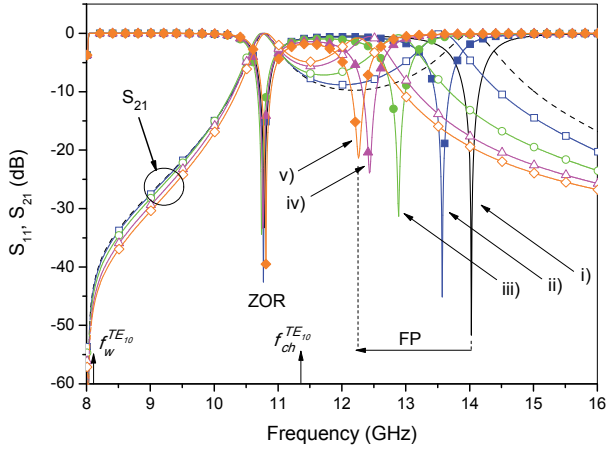


Fig. 18. Influence of a single centered slot angle of inclination on ZOR and FP ( $a_s=5$  mm,  $b_s=0.2$  mm). i)  $S_{11}$ , no slots, ii)  $S_{11}$ , angle  $20^\circ$ , iii)  $S_{11}$ , angle  $40^\circ$ , iv)  $S_{11}$ , angle  $60^\circ$ , v)  $S_{11}$ , angle  $80^\circ$ ;  $S_{21}$  curves are denoted using dashed lines with appropriate symbols

Fig. 20 depicts  $\rho$  parameter versus frequency for this type of slot in the ENZ channel. It can be observed that the radiation losses are pronounced only at FP and not at the tunneling frequency, which was expected since this slot influences only the FP resonance. Also, it can be seen that radiation losses are about a hundred times greater in this case than in both of the previous cases. But, since radiation losses are below 20% of the input power, the transmission coefficient  $S_{21}$  is reduced for less than 1 dB as can be seen in Fig. 18.

## VI. CONCLUSION

In this paper we present novel methods for both simultaneous and separate tuning of the ENZ waveguide resonant frequencies using short slots. We investigate the influence of slot offset in longitudinal slots and slot angle in inclined slot on frequency tuning of the ZOR and FP resonances, respectively. Two longitudinal slots cut at the channel inputs can tune both the ZOR and FP resonances toward lower frequencies. Interesting results are obtained if a single slot is placed in the middle of the channel. Namely, by keeping the slot in the longitudinal form one can manipulate the position of the tunneling frequency merely by changing the slot offset.

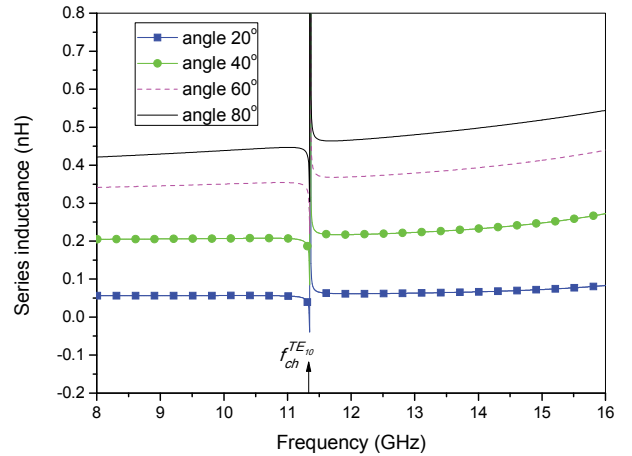


Fig. 19. Frequency dependence of the extracted slot series inductance for four different centered slot angles of inclination

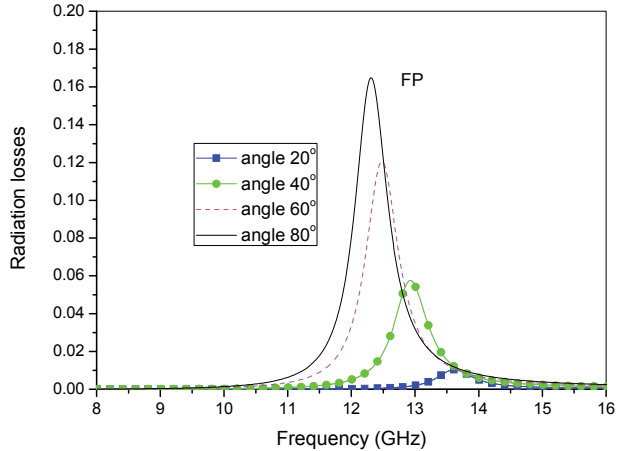


Fig. 20. Dependence of radiation losses on the angle of inclination of the centered slot

In addition, if the slot is rotated with respect to the channel centerline, only the position of the FP resonance is changed. It is shown that the longitudinal offset slot can be represented using an equivalent shunt capacitor, while the rotated slot can be represented using an equivalent series inductor. Based on the extracted equivalent capacitance of the tuning slots, we proposed closed-form expressions that predict very precisely the longitudinal slot capacitance versus frequency for different slot offsets.

### ACKNOWLEDGEMENT

This work was financed by the Serbian Ministry of Education, Science and Technological Development through the projects TR-32024 and III-45016.

This is an extended version of the paper “Independent Resonance Tuning in Rectangular ENZ Waveguide” presented at the 59th Conference for Electronics, Telecommunications, Computers, Automatic Control and Nuclear Engineering - ETRAN 2015, held in June 2015 in Silver Lake, Serbia. The paper has been awarded as the best paper presented in Section Microwave Technique, Technologies and Systems.

### REFERENCES

- [1] W. Rotman, "Plasma Simulation by Artificial Dielectrics and Parallel-Plate Media", *IRE Trans. Antennas and Propag.*, vol. 10, 1962.
- [2] M. G. Silveirinha, N. Engheta, "Theory of Supercoupling, Squeezing Wave Energy, and Field Confinement in Narrow Channels and Tight Bends Using  $\epsilon$  near-zero Metamaterials", *Phys. Rev. B*, vol. 76, 245109, 2007.
- [3] B. Edwards, A. Alù, M. E. Young, M. G. Silveirinha, N. Engheta, "Experimental Verification of Epsilon-Near-Zero Metamaterial Coupling and Energy Squeezing Using a Microwave Waveguide", *Phys. Rev. Lett.*, vol. 100, 033903, 2008.
- [4] D. A. Powell, A. Alù, B. Edwards, A. Vakil, Y. S. Kivshar, N. Engheta, "Nonlinear Control of Tunneling Through an Epsilon-Near-Zero Channel", *Phys. Rev. B*, vol. 79, 245135, 2009.
- [5] M. Mitrović, B. Jokanović, N. Vojnović, "Wideband Tuning of the Tunneling Frequency in a Narrowed Epsilon-Near-Zero Channel", *IEEE Antennas Wirel. Propag. Lett.*, vol. 12, 2013.
- [6] M. Mitrović, B. Jokanović, N. Vojnović, "Experimental Verification of Wideband Tuning of the Tunneling Frequency in ENZ Channel", at the *Metamaterials 2012: 6th Int. Congr. Advanced Electromagnetic Materials in Microwaves and Optics*, St. Petersburg, Russia, Sept. 2012.
- [7] N. Marcuvitz, *Waveguide Handbook*, New York, USA, McGraw-Hill, 1951.
- [8] <http://www.ansys.com>
- [9] N. Vojnović, B. Jokanović, M. Mitrović, "Modeling of Tunneling Effects in Epsilon-Near-Zero Waveguide", *Microw. Rev.*, vol. 18, pp 21-27, 2012.
- [10] N. Vojnović, B. Jokanović, M. Mitrović, F. Mesa, F. Medina, "Tuning ZOR in Epsilon-Near-Zero Waveguide Using a Single Longitudinal Slot and Equivalet Circuit Parameter Extraction", at the *Metamaterials 2014: 8th Int. Congr. Advanced Electromagnetic Materials in Microwaves and Optics*, Copenhagen, Denmark, Sept. 2014.